Nanoscale

PAPER

View Article Online
View Journal | View Issue

Cite this: *Nanoscale*, 2021, **13**, 5507

pH and redox triggered doxorubicin release from covalently linked carbon dots conjugates

Sajini D. Hettiarachchi,[a] Emel Kirbas Cilingir,[a] Heidi Maklouf,[b] Elif S. Seven,[a] Suraj Paudyal,[a] Steven Vanni,[b] Regina M. Graham[b,c] and Roger M. Leblanc *[a]

Tumor microenvironment responsive drug delivery systems are potential approaches to reduce the acute toxicity caused by high-dose cancer chemotherapy. Notwithstanding the conventional nano-drug delivery systems, the redox and pH stimuli drug delivery systems are currently gaining attention. Therefore, the current study was designed to compare three different covalent carbon dots (C-dots) systems based on doxorubicin (dox) release profiles and cancer cell viability efficacy under acidic and physiological conditions. The C-dots nanosystems that were examined in this study are directly conjugated (C-dots-dox), pH triggered (C-dots-HBA-dox), and the redox stimuli (C-dots-S–S-dox) conjugates. The drug loading content (DLC%) of the C-dots-S–S-dox, C-dots-HBA-dox, and C-dots-dox was 34.2 ± 0.4, 60.0 ± 0.3, and 70.0 ± 0.2%, respectively, that examined by UV-vis spectral analysis. The dox release paradigms were emphasized that all three conjugates were promisingly released the dox from C-dots faster in acidic pH than in physiological pH. The displayed highest dox released percentage in the acidic medium was 74.6 ± 0.8% obtained by the pH stimuli, C-dots-HBA-dox conjugate. When introducing the redox inducer, dithiothreitol (DTT), preferentially, the redox stimuli C-dot-S–S-dox conjugate demonstrated a faster dox release at acidic pH than in the pH 7.4. The SJGBM2 cell viability experiments revealed that the pH stimuli, C-dots-HBA-dox conjugate, displayed a significant cell viability drop in the artificially acidified pH 6.4 medium. However, in the physiological pH, the redox stimuli, C-dots-S–S-dox conjugate, was promising over the pH stimuli C-dots-HBA-dox, exhibiting cell viability of 60%, though its' efficacy dropped slightly in the artificially acidified pH 6.4 medium. Moreover, the current study illustrates the stimuli conjugates' remarkable efficacy on sustain drug release than direct amide linkage.

Received 24th November 2020,
Accepted 26th February 2021

DOI: 10.1039/d0nr08381j

rsc.li/nanoscale

1. Introduction

The development of drug delivery systems for cancer pathology has been gradually implemented using various nano-moieties. Over the past few decades, the targeted nano-drug delivery platforms have been recognized as promising treatment methods to overcome conventional chemotherapy obstacles.[1–3] To avoid the severe side effects of nano-motifs, the use of biocompatible and biodegradable materials is predominantly essential.[4] Thus, the carbon dots (C-dots) are superior candidates for the nontoxic drug delivery systems. Carbon dots are multifunctional nanomaterials that enable bioimaging, targeted drug delivery, and multiple drug loading facility. The characteristically unique features that made C-dot a rising star in nanomedicine are excellent biocompatibility, non-toxicity, smaller size (less than 10 nm), and wavelength-dependent/independent emission.[5–8] However, C-dots' potential use in pH or redox triggered systems are limitedly reported up to date. Thus, in this study, we engineered to optimize the sustained drug release by three different nanosystems that are covalently linked to carbon dots.

Targeted drug delivery systems enhance drug carriers' cellular internalization through a specific interaction between targeting ligands and corresponding receptors on the tumor surface. However, the targeted drug delivery approaches have two main disavantages: (1) The targeting ligands can be recognized by endothelial cells directly or through opsonins, which induces the clearance of nanoparticle systems by the blood circulation.[9,10] (2) The corresponding receptors for the targeting ligands are not expressed only by tumor cells but also by the healthy cells, which ultimately can cause side-effects to healthy cells.[11] Therefore, parallel to the targeted drug delivery systems, the researchers tend to explore new nano-therapeutic strategies to minimize acute toxicity. The drug delivery systems could be designed to acquire sustained drug release by

[a]*Department of Chemistry, University of Miami, 1301 Memorial Drive, Coral Gables, Florida, 33146, USA. E-mail: rml@miami.edu*
[b]*Department of Neurological Surgery, University of Miami, Miller School of Medicine, Miami, Florida 33136, USA*
[c]*Sylvester Comprehensive Cancer Center, University of Miami Miller School of Medicine, 1475 NW 12th Ave, Miami, FL 33136, USA*

responding to a particular stimulus such as temperature, ultrasound intensity, magnetism, redox, and pH.[12–14] Among all the incentives, the pH or redox-sensitive drug release systems have significant potential to enhance the therapeutic efficacy due to the existing pH differences between normal physiological pH and acidic tumor microenvironment as well as the concentration differences of the reducing agent glutathione (GSH).[15]

The propensity of tumors to invade acidic microenvironments is due to the fast cell proliferation. The higher proliferation rate tends to increase glucose uptake and metabolism, leading to enhanced lactate and H^+ production.[16] The high production and export of H^+ ions in tumors result in an acidic extracellular microenvironment in malignant tumors compared to healthy cells.[17] During the tumor progression, the highly produced H^+ ions flow through a concentration gradient from tumor tissues into healthy tissues resulting in a tumor remodeling in the tumor-stroma interface.[18] As a result, the toxic acidic environment causes the degradation of the healthy extracellular matrix by proteinases and ultimately inhibits the immune response to tumor antigens.[19,20] Consequently, when a healthy cell dies, the extracellular matrix will deteriorate, resulting in tumor cells' occupation and proliferation in this open space. Finally, the enhanced evolutionary capacity and adaptive nature of the tumor cells dominate while enhancing the survival and proliferation within the acidic environment.[21]

Glutathione (GSH) is a reducing agent and an antioxidant found in the cytosol and a tripeptide made up of glutamate, cysteine, and glycine. GSH is more prominent in acting as a reducing agent than an antioxidant, and 1–15 mM concentration can be found in cells. GSH prevents the cellular damage caused by reactive oxygen species (ROS) such as free radicals and peroxides.[22] Glutathione involves many physiological actions, including cancer cell death *via* apoptosis, necrosis, and autophagy.[23] As a result, elevated levels of GSH concentration can be found in tumor cells.[24,25] However, as a constraint of the elevated levels of GSH, the cancer cell becomes resistant to chemotherapeutic agents such as doxorubicin and platinum compounds. Despite all the physiological roles of GSH, it is also known to be involved in disulfide bond reduction of native proteins and non-native proteins resulting from oxidative stress.[26,27]

Among the most popular hydrolytically labile bonds, such as imine, oxime, acetal, or orthoester, the hydrazone bond was specific due to its' responsive acuteness and the facile conjugation ability on C-dots.[28,29] According to the previous studies, the faster drug release rate with the hydrazone linkage was observed in the pH range of 5–6.[30] Even though the hydrazone bond is widely used in nanoparticles and polymeric pH-responsive systems, C-dots nanoplatforms are minimal.[31–34] Yang *et al.* have used the hydrazone bond to fasten the dox on amine-functionalized C-dots and reported promising results on low pH dox release rates.[34] Yang *et al.* reported that the hydrazone bond linked dox was released from the C-dots faster at pH 5.5 than at 7.4. However, the study was not considered the effect of redox conditions on the hydrazone bond cleavage. Thus, in the current study, we examined the effect of redox conditions on pH stimuli conjugate. Even though the redox stimuli, drug release systems are widely popular in polymer nanosystems, pointedly low in C-dots.[27,35,36] Chen *et al.* was reported a redox responsive dox delivery system of a nanoporous silica system.[37] They illustrated the higher efficacy of the disulfide cleavage and dox release rates under the conditions of 10 mM GSH at pH 5.0.[37] Hence, we introduce the redox stimuli system for the nontoxic C-dots and investigate the efficacy under DTT mediated acidic and physiological conditions as well as in cell media.

Over the past few years, we have reported the black C-dot as a promising drug delivery nanomotif, which can undergo covalent attachments.[6,8] The current study focuses on the comparative analysis of drug release profiles, of three different covalently bonded C-dots conjugates, under the stimuli conditions (pH and redox). Subsequently, the efficacy in the glioblastoma brain tumor cell-line, SJGBM2, was analyzed. Dox was covalently conjugated onto C-dots *via* an acid-labile hydrazone linkage and a redox stimuli disulfide linkage (Fig. 1). The pH stimuli C-dots nanosystem was synthesized by covalently conjugating dox onto C-dots *via* acid-sensitive hydrazone linkage using hydrazinobenzoic acid (HBA). The redox stimuli carbon dots system was synthesized by conjugating dox on C-dots through S–S bond using 3-[(2-aminoethyl)dithio]propionic acid. HCl (AEDP). pH and redox stimuli conjugates were compared to the direct conjugated C-dots-dox conjugate.

2. Materials

Carbon nanopowder (<100 nm), 4-hydrazinobenzoic acid (HBA), *N*-hydroxy succinimide (NHS), 1-ethyl-3-(3-dimethyl aminopropyl) carbodiimide hydrochloride (EDC), dithiothreitol (DTT), and lactic acid were bought from Sigma Aldrich (St Louis, MO). ACS grade sulfuric acid (98%) and nitric acid (68–70%) were obtained by ARISTAR (distributed by VWR, Radnor, PA). ThermoFisher Scientific (Waltham, MA, USA) provided the dialysis tubing with molecular weight cutoff (MWCO) 3500 Da, and the (3-[(2-aminomethyl) dithiolpropionic acid) (AEDP). Doxorubicin hydrochloride was bought from TCI chemicals (Portland, OR, USA). The de-ionized (DI) water purification system, MilliQ3 was purchased from MilliporeSigma (Burlington, MA) which has a resistivity of 18 MΩ·cm and surface tension of 72.6 mN m^{-1} at 20.0 ± 0.5 °C. The pediatric brain tumor cell line, SJGBM2, was procured from Childrens' Oncology Group (COG, Lubbock, TX). Cell lines were cultured in RPMI-1640 (ThermoFisher Scientific, Waltham, MA, USA) and supplemented with 10% heat-inactivated fetal bovine serum and 1% penicillin–streptomycin, which were purchased from Gemini Biosciences (West Sacramento, CA). LookOut mycoplasma PCR detection kit from Sigma Aldrich (St Louis, MO) was used to routinely test all the cell lines per the manufacturers' instructions and maintained at 37 °C in a humidified 5% CO_2 incubator.

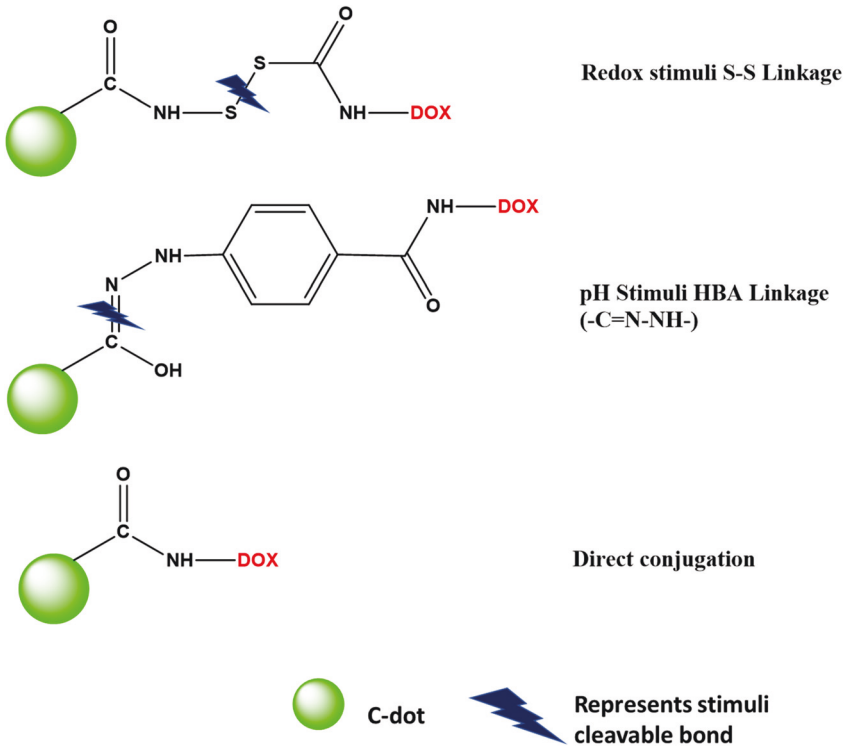

Fig. 1 Schematic illustration of the bond anatomy of each conjugate. The diagram represents only the 1 : 1 : 1 ratio of the C-dot: stimuli linkage: dox.

3. Methodology

3.1. Synthesis of carbon dots

Carboxylic acid-functionalized C-dots were synthesized by following Li *et al. via* the acidic oxidation.[38] In brief, carbon nanopowder, 1 g was mixed with sulfuric acid (36 mL) and nitric acid (12 mL) in a round bottom flask. The mixture was refluxed for 15 h at 110 °C in an oil bath. After the reflux, the mixture was cooled down to room temperature, and the unreacted acids were neutralized by using a saturated sodium hydroxide solution (pH 14). The neutralization was carried out in an ice bath. The mixture was vacuum filtered to remove the unreacted carbon powder, and the supernatant was kept in an ice bath to precipitate the unwanted salts. A piece of sodium sulfate was added to avoid the super-saturation. The step of unwanted salt filtration was repeated twice. The mixture was followed by washing with chloroform (60 mL) three times to remove organic wastes. The purified solution was centrifuged at 3000 rpm for 30 minutes. The centrifuged solution was transferred to a 3500 Da molecular weight cut off (MWCO) dialysis membrane and dialyzed against 4 L of de-ionized water for 5 days while replacing the water for every 4–10 h. Finally, the purified C-dots solution was placed in the rotovap to evaporate off the water and acquire the powdered C-dots.

3.2. Synthesis of pH stimuli, C-dots-HBA-dox

The covalent conjugation of acid-sensitive HBA and C-dots was initiated by dissolving 8 mg of C-dots in 2 mL of PBS. Then 4 mL of HBA/DMSO solution (9.5 mg mL^{-1}) was added into the C-dots solution. A drop of glacial acetic acid was added to acidify the reaction medium. The reaction mixture was stirred at room temperature for 72 h. The solution was then transferred into a 3500 Da MWCO dialysis membrane and dialyzed for three days against de-ionized water. The purified C-dots-HBA solution was transferred into a round bottom flask for the conjugation of dox. The 1 mL of EDC/PBS solution (17.7 mg mL^{-1}) was added into the purified C-dots-HBA solution, and after 30 min, 1 mL of NHS/PBS solution (10.68 mg mL^{-1}) solution was followed. Later in 30 min, the dox/DMSO (4.72 mg mL^{-1}) solution was added to the mixture. The mixture was stirred overnight and followed by the dialysis for three days using the 3500 Da MWCO dialysis membrane. After the purification, the solution was frozen at −80 °C and lyophilized to obtain the powdered C-dots-HBA-dox conjugate.

3.3. Synthesis of redox stimuli, C-dots-S–S-dox

An 8.0 mg of C-dots was dissolved in 2 mL of PBS. The EDC/PBS solution (17.7 mg mL^{-1}) was added to the C-dot solution, and 30 min later, 1 mL of NHS/PBS solution (10.68 mg mL^{-1}) was introduced. The 1 mL of AEDP/DMSO solution (6 mg mL^{-1}) was added after 30 min. The mixture was stirred overnight and purified for 3 days by using the 3500 Da MWCO dialysis membrane. After the purification, the C-dots-AEDP conjugate was reacted with dox *via* the EDC/NHS coupling conjugation method. The same amount of EDC and NHS was added, as described in section 3.1. The dox/DMSO solution

(4.72 mg mL^{-1}) was introduced to the mixture after 30 min of NHS addition. The mixture was stirred overnight and purified with de-ionized water by using the 3500 Da MWCO dialysis membrane. The purified solution was frozen at −80 °C and then lyophilized to obtain the powdered redox stimuli, C-dots-S–S-dox conjugate.

3.4. Synthesis of directly conjugated, C-dots-dox

The C-dot-dox conjugate synthesis was initiated by dissolving 8.0 mg of C-dots in 2 mL of PBS solution. As mentioned in 3.1, the EDC and NHS were added in the same amounts at the same time intervals. The 4.72 mg of doxorubicin (pre-dissolved in 1 mL of DMSO) was introduced into the mixture 30 min later of the NHS's addition. The solution was stirred overnight and dialyzed by using the 3500 Da MWCO dialysis membrane. The powdered C-dots-dox conjugate was obtained by the freeze-drying technique.

3.5. *In vitro* drug release

3.5.1 pH effect. The dialysis technique was used to analyze the release profile of doxorubicin from C-dots conjugates at pH 7.4 and 5.5, respectively. The nano-complexes (2 mg) were dispersed in 2 mL PBS and then were sealed in a dialysis membrane. Each dialysis membrane was immersed in 30 mL of PBS solutions at each pH. Subsequently, the dialysis membranes were continuously stirred at 37 °C. A 1 mL of the PBS was withdrawn from the bulk solution at specific time intervals while replacing it with 1 mL of fresh PBS from the relevant pH. The released doxorubicin concentration was quantified by the UV-vis spectroscopic absorptions at 480 nm.

3.5.2 Redox effect. Cumulative doxorubicin release percentages were quantified using the dialysis technique at each pH in the presence of DTT, which mimics the glutathione in biological systems. As mentioned in section 3.4.1, the nano-complexes (2 mg) were dispersed in 2 mL PBS and then were sealed in a dialysis membrane. Each dialysis membrane was immersed in 30 mL of PBS solutions at each pH. Each PBS solution at each pH was mixed with DTT at a final concentration of 5 mM. Afterward, the dialysis membranes were continuously stirred at 37 °C, at specific time intervals, 1 mL of the PBS was withdrawn from the bulk solution while replacing it with the same amount of fresh PBS from the relevant pH. The released doxorubicin concentration was quantified by the UV-vis spectroscopic absorptions at 480 nm.

3.6. Cell viability

The pediatric brain tumor cell line, SJGBM2, was plated in 96 well plate with 1×10^4 cells per well, 24 h prior to the drug treatment. Subsequently, the cells were treated with 0.1 μg mL^{-1} of conjugates at physiological pH 7.4 and acidic pH 6.4 media. The cell medium was artificially acidified to obtain pH 6.4 by introducing 6 μL of lactic acid (0.5 M) into each well. Cells were treated with drug conjugates for 6, 24, or 72 h, and viability determined by the MTS method. For the 6 and 24 h periods, media/drug conjugate was removed and replaced with fresh media, and viability was determined at 72 h from the start of the experiment. Additionally, the cells were treated for 6 h under acidic conditions, and the media was replaced with fresh pH 7.4 buffer solution. Subsequently, the viability was determined after 72 h, using CellTiter 96® Aqueous One Solution Cell Proliferation Assay (Promega) based on the manufacturer's instructions. Absorbance was measured at 490 nm using a BioTek Synergy HT Plate reader. The represented data is an average of three consecutive sets of experiments, and the viability was calculated as the percent of non-treated cells. Significance was determined using the Students *T*-test. Different batches of C-dots-conjugates confirmed the consistency of the data.

4. Characterization

The synthesized conjugates (20 μg mL^{-1}) were analyzed in a 1 cm quartz cell using a UV-vis spectrometer of Shimadzu UV-2600. The fluorescent emission spectra of the conjugates were recorded by Horiba Jobin Yvon Fluorolog-3 using a slit width of 5 nm for excitation and emission. The FTIR analysis was performed on a PerkinElmer FTIR (Frontier) spectrometer using the attenuated total reflection (ATR) technique. Each characterization technique was repeated with three different batches of C-dots-conjugates to verify the consistency of the data and the stability of the conjugates.

5. Results and discussion

Stimuli conjugates were synthesized by two-step reactions, whereas the C-dots-dox direct conjugation was a one-step reaction. The C-dots-HBA-dox conjugate synthesis was initiated by linking the carboxylic group (–COOH) of C-dot covalently with the hydrazine group (–NH–NH_2) of HBA. Subsequently, as the second step, the carboxyl terminus of the HBA was coupled covalently to the primary amine of the dox to form the complete pH stimuli, C-dots-HBA-dox conjugate. The synthesis of redox stimuli, C-dots-S–S-dox, was initiated by linking the amine terminal of AEDP to the –COOH group of C-dots, and in the second step, the dox was conjugated on the –COOH terminal of the AEDP. Both the ends of the AEDP were linked *via* the EDC/NHS amide covalent coupling. The C-dox-dox direct conjugation was synthesized by conjugating the primary amine group of dox on the –COOH group on C-dots *via* the EDC/NHS coupling addition reaction. The conjugates were characterized by UV-vis, fluorescence, and FTIR spectroscopy.

5.1. UV-vis and fluorescence spectroscopic analysis

The conjugates were characterized by the UV-vis and fluorescence spectroscopies to verify the successful conjugation of each linker and dox on C-dots. The presence of doxorubicin in the conjugates of C-dots-S–S-dox and C-dots-dox was exhibited by the characteristic doxorubicin absorption band 480 nm (Fig. 2b and c), whereas in the C-dots-HBA-dox spectrum, the doxorubicin peak was blue-shifted to 370 nm (Fig. 2a). The

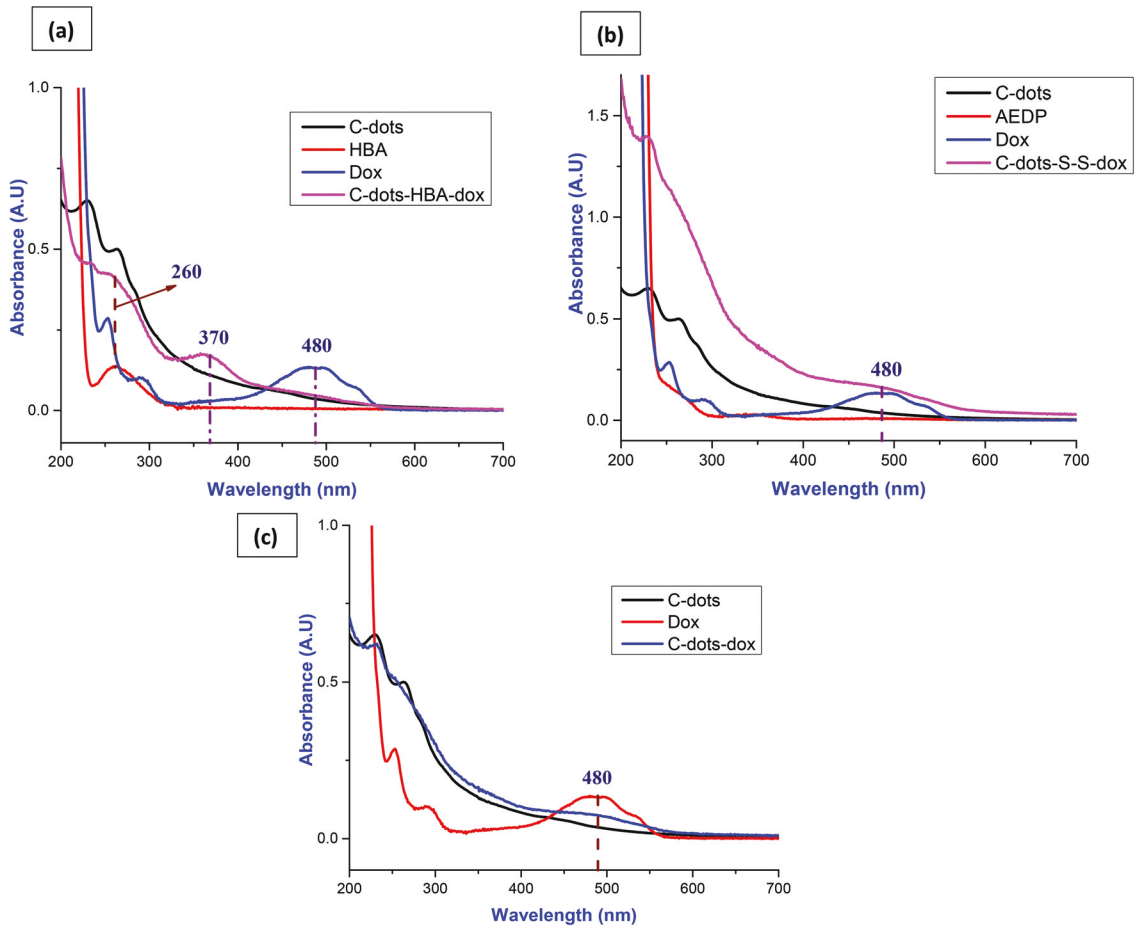

Fig. 2 The UV-vis absorption spectral analysis of (a) C-dots-HBA-dox (b) C-dots-S–S-dox and (c) C-dots-dox. The 20 μg mL^{-1} samples were analyzed in a 1 cm quartz cell.

successful HBA conjugation on C-dots was exhibited by the band overlap of free HBA and C-dots-HBA-Dox spectrums at 260 nm (Fig. 2a). The presence of S–S linkage on C-dots was challenging to convince by the UV-vis spectral analysis due to the UV inactiveness of AEDP. Hence the successful conjugation of the S–S linker was confirmed by the FTIR spectral analysis.

The loaded doxorubicin concentration in each C-dot conjugate was analyzed by the UV-vis spectroscopy. The prominent excitation of dox was detected at 480 nm; hence, the dox was quantitatively assayed according to a calibration curve. The drug loading content (DLC) was calculated by the following formula:

$$\text{DLC } \% = \frac{\text{Amount of dox conjugated on to C-dots}}{\text{Total amount of the conjugate}} \times 100$$

Triplicate UV-vis absorption measurements were carried out from three different batches, and the average DLC% of the C-dots-S–S-dox, C-dots-HBA-dox, and C-dots-dox were 34.2 ± 0.4, 60.0 ± 0.3, 70.0 ± 0.2%, respectively.

The fluorescence spectroscopic analysis was also determined by the successful conjugation of dox on C-dots. Dox characterizes a couple of wavelength-independent emissions peaks at 558 and 591 nm. The successful conjugation of the dox was revealed by the appearance of typical dox bands in each conjugates' emission spectrum (Fig. 3a–c). Despite the dox bands, the successful conjugation of HBA on C-dots was also confirmed by the fluorescence spectral analysis. The characteristic HBA band appeared at 391 nm (Fig. 3a) in the C-dots-HBA-dox conjugate spectrum, which has 38 nm red-shifted than the free HBA fluorescence band (Fig. 3d).

5.2. FTIR spectroscopic analysis

The FTIR spectrum of C-dots-HBA-dox exhibited the successful conjugation of HBA on C-dots by the appearance of C=N hydrazone vibration at 1692 cm^{-1} (Fig. 4a). However, according to the literature, the characteristic C=N band for free HBA appears at 1662 cm^{-1}. The slight deviation of the HBA band position in the C-dots-HBA-dox spectrum can be attributed to the possibility of having new intermolecular interactions than the free HBA.[39] A strong S–S stretching band was observed at the 546 cm^{-1} in the C-dots-S–S-dox conjugate (Fig. 4b and c). Though the S–S band position of the conjugate depicted a minor deviation from the AEDP S–S band position, the deep band topology confirmed the successful conjugation of AEDP

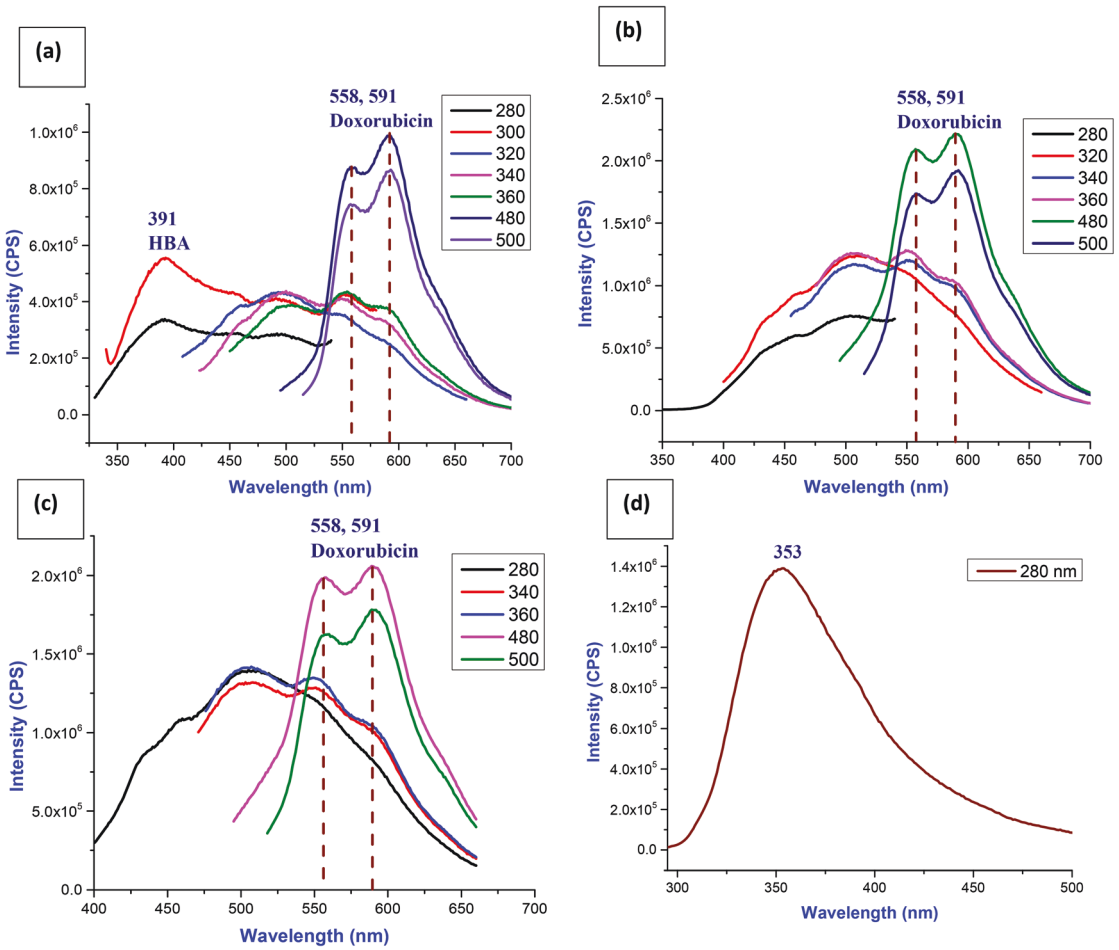

Fig. 3 The fluorescence emission spectral analysis of (a) C-dots-HBA-dox, (b) C-dots-S–S-dox, (c) C-dots-dox, and (d) free HBA. The samples (10 μg mL^{-1}) were tested in a 5 nm slit width for excitation and emission.

on C-dots. Therefore, the FTIR spectral analyses were promisingly confirmed the successful conjugation of HBA and the AEDP on C-dots in each conjugate.

5.3. *In vitro* drug release

The amount of dox loaded onto each C-dots motifs was quantitatively measured by using the UV-vis spectroscopic analysis. The absorbance at 480 nm was measured in each conjugate and calculated the percent DLC by a calibration curve. The average DLC% for C-dots-S–S-dox, C-dots-HBA-dox, and C-dots-dox was 34.2 ± 0.4, 60.0 ± 0.3, and 70.0 ± 0.2%, respectively. The Dox release efficacy was investigated at pH 7.4 and 5.5 in the presence or absence of DTT. The disulfide bond cleavage induces chemically by DTT, which mimics the GSH in the biological system.

5.3.1. *In vitro* drug release (absence of DTT). C-dot conjugates were dissolved in PBS and sealed in dialysis membranes. The sealed samples were dipped in pH 7.4 and 5.5 PBS mediums at 37 °C for 25 h. At specific time intervals, 1 mL of solution was withdrawn while replacing it with fresh PBS. The cumulative dox release paradigms were plotted using the UV-vis spectroscopic analysis, and each point represents the average of triplicate measurements (Fig. 5).

Markedly, the dox release rates for all the conjugates were faster under acidic conditions (pH 5.5) than in pH 7.4. Compared to the three conjugates' dox release behaviors in the acidic medium, obviously, the pH triggered C-dots-HBA-dox conjugate depicted faster and the highest cumulative dox release percentages over the 25 h period. The displayed highest cumulative dox released was 74.6 ± 0.8% by C-dots-HBA-dox conjugate in the acidic condition, whereas it was 52.4 ± 1.1% in the physiological pH 7.4 (Fig. 5). This demonstrates the significant hydrolysis efficiency of hydrazone bonds in acidic conditions. Hydrozones bonds tend to release the covalently bound payload in lower pH due to the imine nitrogen protonation. Therefore, preferentially the pH stimuli conjugate was significantly promising than the other two conjugates in the acidic medium.

Notably, the second-highest cumulative dox release percentage was displayed by C-dots-S–S-dox under the acidic conditions. A 66.3 ± 1.0% of dox was released from the C-dots-S–S-dox in the acidic medium, whereas 47.6 ± 1.9% was released in

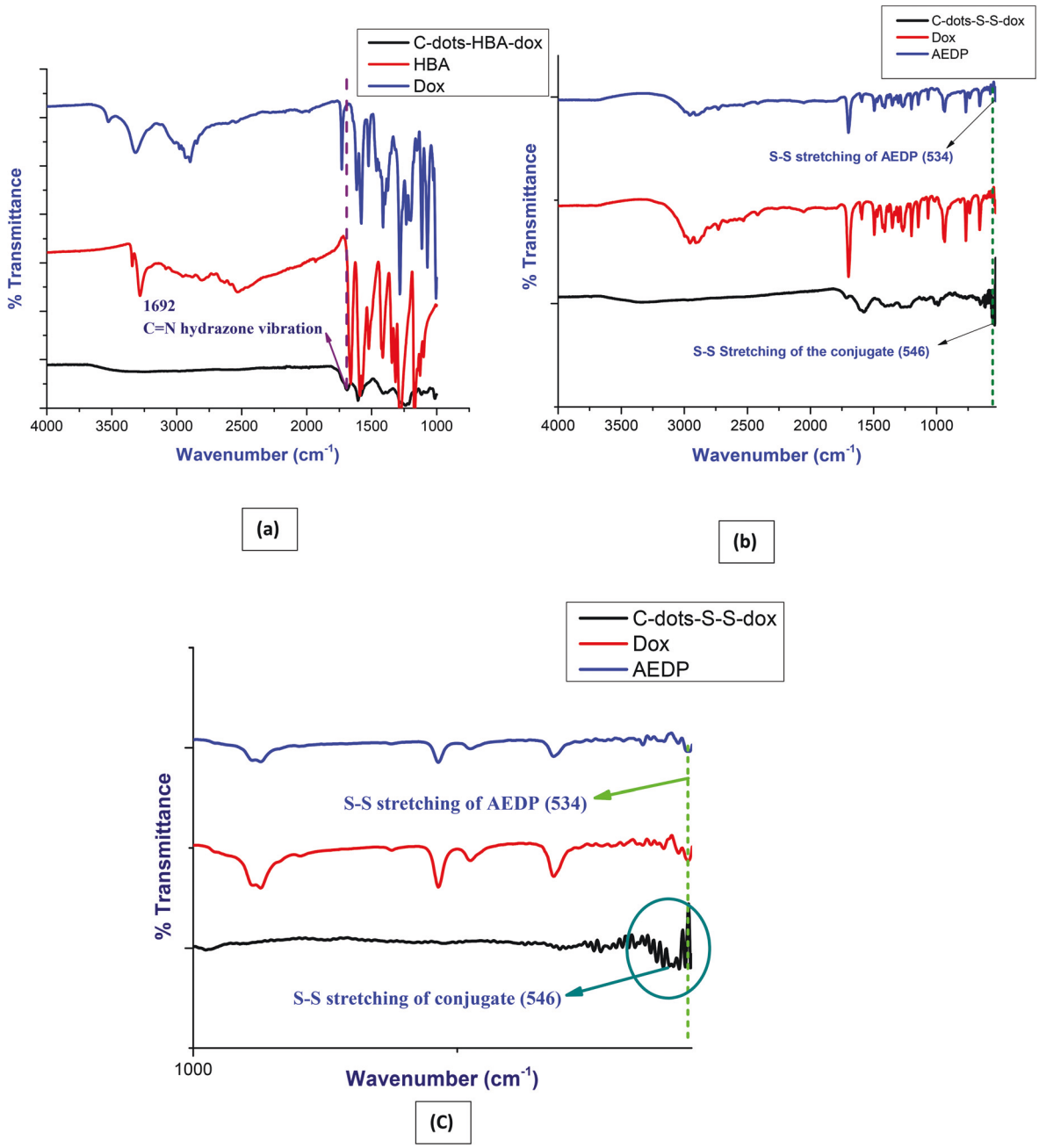

Fig. 4 The FTIR spectral analysis comparison of (a) C-dots-HBA-dox, dox, and HBA, (b) C-dots-S–S-dox, AEDP, and dox (c) the enlarged figure of C-dots-S–S-dox conjugate.

the pH 7.4 (Fig. 5). The correlation between pH and disulfide bond stability explains the likelihood of S–S bond cleavage in the acidic medium. The stability of the disulfide bond favors the neutral or basic pH, and conversely, at the acidic pH, the stability hinders, resulting in the obligation into the thiol formation.[40] Thus, not only the pH stimuli conjugate but the redox stimuli conjugate also comparably significant in the acidic medium even in the absence of DTT.

The observed lowest cumulative dox release percentage over 25 h period was 31.3 ± 0.9% displayed by the directly conjugated C-dots-dox conjugate in the acidic medium, and the 22.6 ± 1.1% was in the neutral pH (Fig. 5). This emphasizes that the pH and redox stimuli conjugates are highly susceptible to labile under acidic conditions than the direct conjugation. Even though the direct amide covalent linkage is more vital not to cleave under acidic or physiological conditions, the low percentage of dox release in this study can be explained by the previously reported pH corresponded amide bond hydrolysis. The amide bond is highly stabilized when only forming the planer resonance structures. The planar structure hinders

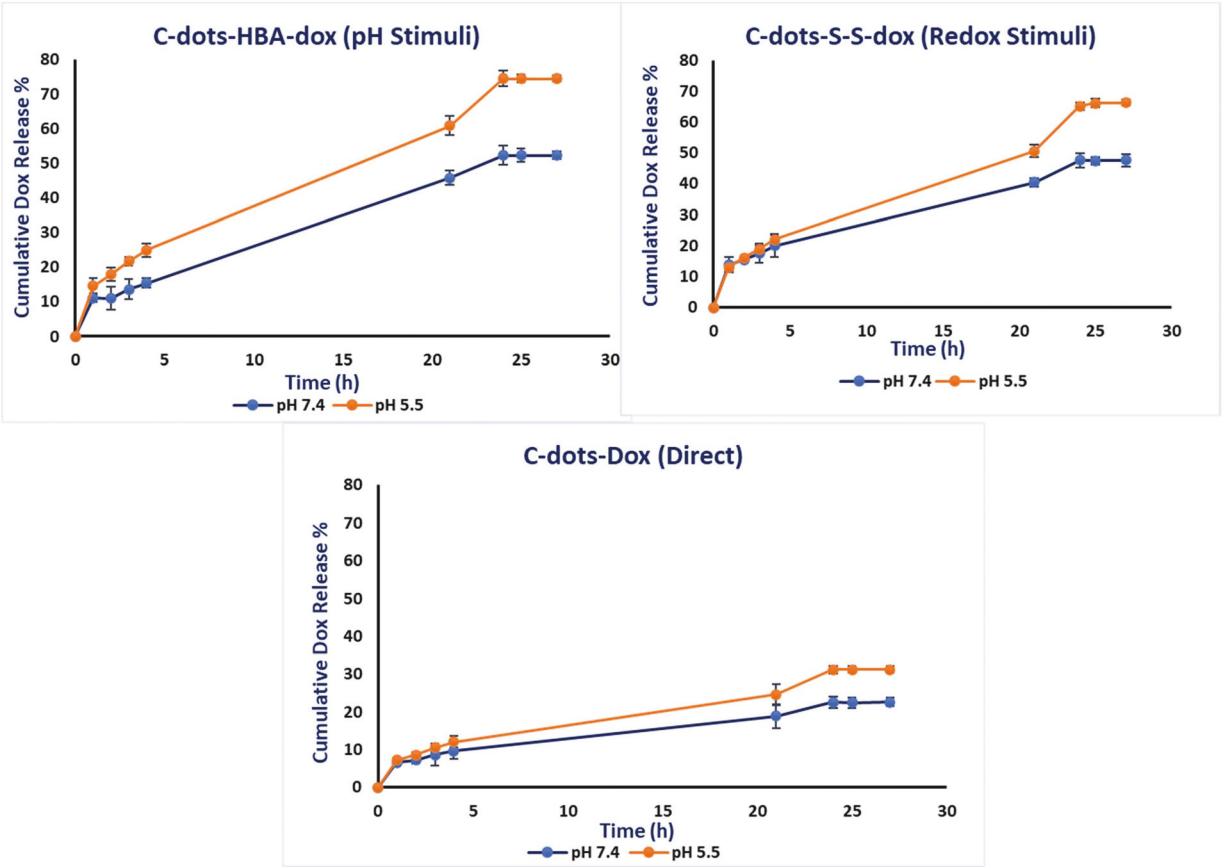

Fig. 5 The cumulative dox release paradigms of C-dots-HBA-dox, C-dots-S–S-dox, and C-dots-dox at pH 7.4 and 5.5. Each data point represents the average of triplicate measurements, and the error bars represent the standard deviation. The data points that do not display the error bars indicate a standard deviation of less than 1.0%.

the free rotation that obstructs nucleophilic or electrophilic attacks.[41] However, the amide bond activation or the cleavage can occur if it forms the inversely rotated or twisted distortion susceptible to nucleophilic or electrophilic attacks. The twisted rotations of the amide bonds have been evidenced widely in cyclic non-planer bulky molecules.[42–44] Thus, in this study, the doxorubicin is a bulky molecule that contains phenyl ring attached $-NH_2$ groups that reacted with the –COOH group of the C-dots. Therefore, while forming the amide covalent bonds, some bonds might be formed as partially distorted or twisted and non-planer, susceptible to electrophilic attacks, which induces the hydrolysis/cleavage of the amide bond for dox to release.[45]

Even though all the three conjugates displayed higher dox release rates in the acidic medium, the pH and redox stimuli conjugates markedly promising to use in tumor microenvironments than the directly conjugated C-dots-dox.

5.3.2. *In vitro* drug release (with DTT). As discussed earlier, the tumor microenvironment does not only low in pH but also rich in GSH concentration. Therefore, we analyzed the conjugates' dox release behavior in the DTT medium. Fig. 6 illustrates the dox release paradigms of each conjugate at two pHs, 7.4, and 5.5 in the presence of DTT. The DTT concentration was 5 mM in each pHs' buffer solution, which approximately mimics the concentration of GSH in healthy human cells. Unlike the dox release rates in the absence of DTT, only the C-dots-S–S-dox displayed a higher dox release percentage in the acidic condition in the presence of DTT. Over the 25 h period, 65.3 ± 2.2 and 71.2 ± 1.1% of dox were released from C-dots-S–S-dox conjugate in the pH 7.4 and 5.5, respectively. The released dox percentages from the redox stimuli, C-dots-S–S-dox, were not considerably different in the acidic and physiological pH. Thus, in both the pHs, rates of disulfide reductive cleavages were likely-comparable, which conclusively suggests that the DTT was stable in both the pHs over the period of 25 h and preferentially, the redox stimuli, C-dots-S–S-dox conjugate, favors the GSH rich environments.

5.4. Cell viability/cytotoxicity

The glioblastoma brain tumor cell line, SJGBM2, was treated with C-dots-HBA-dox, C-dots-S–S-dox, or C-dots-dox under physiological and acidic pH. The cell viability was measured after 6, 24, and 72 h in the physiological pH and after 6 h in the acidic pH 6.4. Fig. 7 elucidates the cell-viability percentages of each conjugate at pH 7.4. The cell viability percentages were elegantly demonstrated that the cytotoxicity enhancement

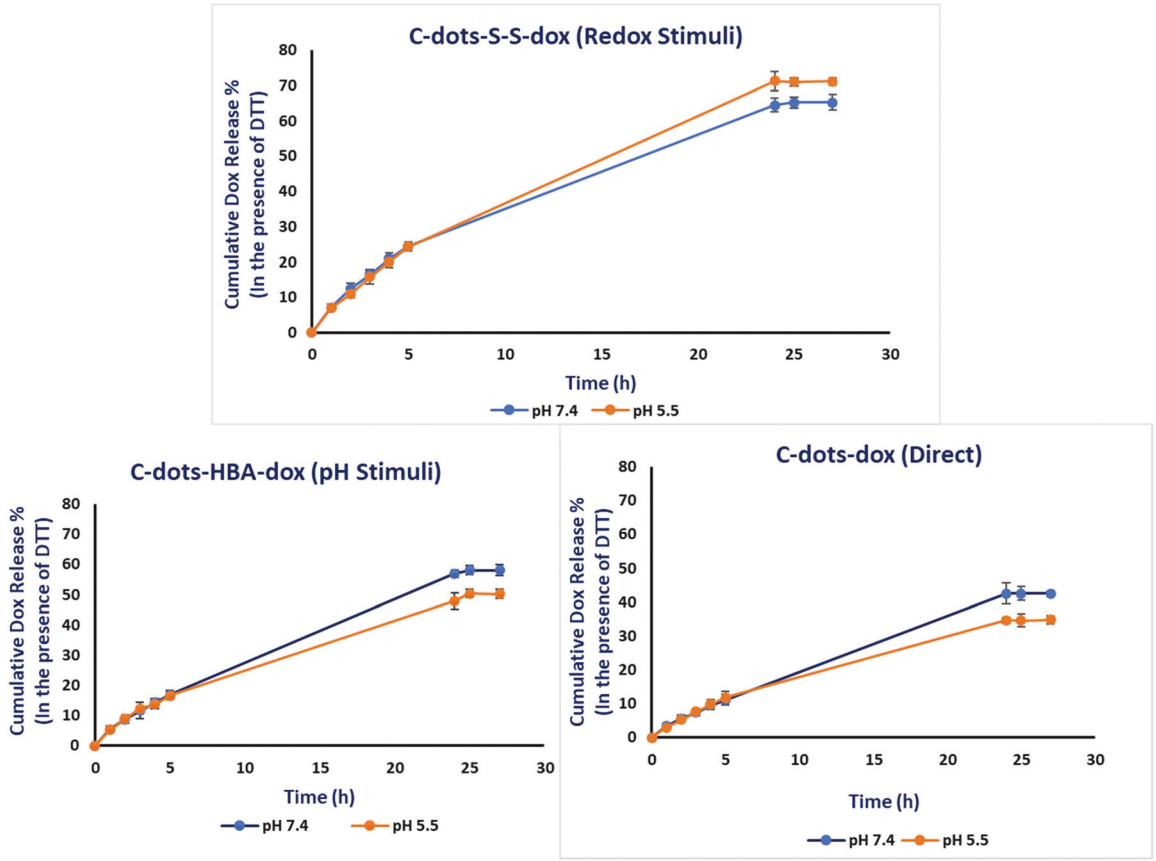

Fig. 6 The cumulative doxorubicin release profile of C-dots-S–S-dox, C-dots-HBA-dox, and C-dots-dox in the presence of DTT at pH 7.4 and 5.5. Each data point represents the average of triplicate measurements, and the error bars represent the standard deviation. The data points that do not display the error bars indicate a standard deviation of less than 1.0%.

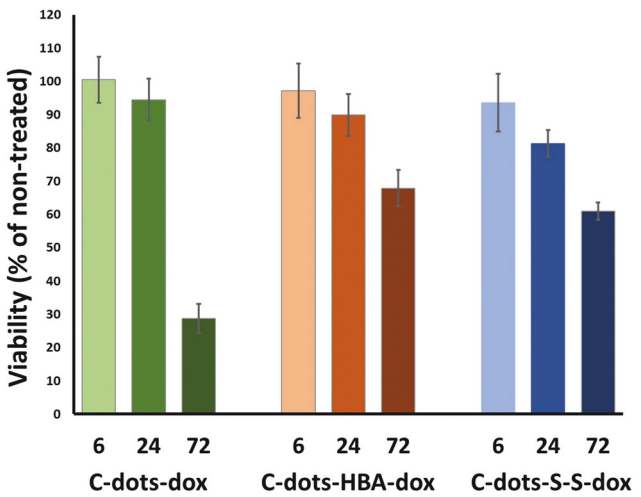

Fig. 7 The cell viability percentages of the cell line, SJGBM2, after treated with each C-dot conjugate. Cells were treated with a concentration of 0.1 μg mL^{-1} of each C-dot conjugate for 6, 24, or 72 h. % cell viability was recorded by comparing to non-treated controls, $*p < 0.05$.

occurred with the incubation time increment. Compared to the redox-stimuli, S–S linkage with the pH-stimuli, HBA linkage, the redox-stimuli, S–S linkage displayed the lowest cell viability 60% after 72 h. In terms of DLC% on each conjugate, the C-dots-S–S-dox conjugate has the lowest DLC% of 34.2. Hence, the C-dots-S–S-dox conjugate is tremendously efficient in depleting the cell viability while having a lower drug amount, which preferentially suggests the possibility of displaying less acute toxicity to healthy cells. GSH/GSSG is the most abundant redox couple in the cell that determines the antioxidant capacity. As explained earlier, when the GSH concentration is higher than GSSG in the cell, the GSH : GSSG ratio will be enhanced.[27] As a result, the chemically degradable disulfide materials can be cleaved through GSH by the GSH-disulfide exchange reaction. Literature *in vivo* experiments demonstrated that the tumor cells contain 4-fold higher GSH concentration than the healthy cells.[46] In facts, even though this current experiment conducts only *in vitro* cell studies, the higher cytotoxicity of C-dots-S–S-dox conjugate than C-dots-HBA-dox conjugate demonstrates that the redox stimuli linkage is better than the pH-stimuli linkage, preferentially due to the presence of higher GSH concentration in the cytosol of the SJGBM2 cell line. Moreover, compared to the cell viabi-

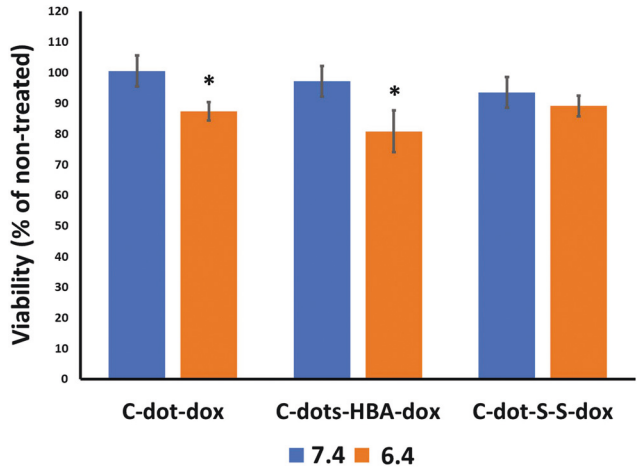

Fig. 8 The cell viability percentages of the cell line SJGBM2, after treated with each conjugate at the concentration of 0.1 μg mL^{-1}. The cell medium was artificially acidified with lactic acid (0.5 M concentration). The cells were incubated with conjugates for 6 h. % Cell viability was recorded by comparing to non-treated controls, $*p < 0.05$.

lity depletion rates of pH and redox stimuli conjugates, both the conjugates displayed a slow rate emphasizing both of the conjugates are superior candidates for sustained drug release. On the other hand, directly conjugated C-dots-dox conjugate exhibited a drastic cell viability drop at 72 h than 24 h, possibly due to the uncontrollable dox release over time. Therefore, the cell viability experiment at physiological pH indicated that only the pH and redox stimuli conjugates are promising for slow, sustained drug release while redox stimuli C-dots-S–S-dox conjugate capable of displaying the lowest cell viability than the pH stimuli conjugate over time.

Naturally, the tumor microenvironments are rich in acidic conditions in the biological systems. However, to proceed with the *in vitro* cell experiments in acidic conditions for an extended period is challenging due to the cell proliferation retardation enhancement. Thus, we examined the cell viability differences of SJGBM2 after treating with each conjugate (0.1 μg mL^{-1} concentration) only for 6 h at the acidic conditions, at which the drug conjugates were removed and replaced with fresh pH 7.4 media. The additional acidity was created in the cell medium by introducing lactic acid, and the pH of the medium was kept at 6.4. Preferentially, the pH stimuli, C-dot-HBA-dox conjugate, displayed a significant cell viability drop, from 18% compared to the pH 7.4 cell viability percentage (Fig. 8). The C-dots-S–S-dox and C-dots-dox conjugates were displayed a 12 and 5% drop, respectively. Surprisingly, the less cytotoxic behavior of the redox stimuli, C-dots-S–S-dox conjugate, may be explained with several reasons. Introducing lactic acid to the medium may enhance the oxidative stress level in the cells, resulting in a higher ROS production. GSH plays a pivotal role in the body as a ROS scavenger.[47] Thus, the present GSH level in the cell could be more likely to participate in the oxidative stress suppression to maintain the cellular redox homeostasis. This process leads to the oxidation of GSH, resulting in the GSSG. Though the reduced GSH could be salvage from GSSG by glutathione reductase (GR), the GR levels are dramatically depleted in the oxidative stress situations. Hence the GSSG deposition can be elevated in the cell by limiting the reduced GSH levels.[48] As a result, the participation of the GSH in the disulfide cleavage could be limited, which leads to the lower anti-cancer activity of the redox stimuli, C-dot-S–S-dox conjugate. However, glutathione monoester is a candidate for an artificial intracellular GSH level enhancer in the *in vitro* experiments, though we have not examined it in this research study.[26]

6. Conclusion

In summary, the dox release behavior of pH and redox stimuli covalent conjugates were compared to direct conjugated C-dot-dox. *In vitro* drug release was illustrated that the pH stimuli, C-dots-HBA-dox conjugate released the maximum cumulative dox amount of 74.6 ± 0.8% at acidic pH in the absence of DTT. In contrast, in the presence of DTT, the redox-stimuli, C-dots-S–S-dox conjugate was displayed the maximum cumulative dox release of 71.2 ± 1.1% in the acidic pH 5.5. The cell viability experiments in the pH 7.4 revealed that the redox and pH stimuli conjugates were promising candidates for sustained slow drug release. However, when the cell medium was artificially acidified to maintain the pH 6.4, only the pH stimuli, C-dots-HBA-dox conjugate, notably dropped the cell viability. The low anti-cancer efficacy of the redox stimuli, C-dots-S–S-dox conjugate might probably be due to the depletion of reduced GSH levels in the cells that, required for the disulfide bond elevation. The redox stimuli, C-dots-S–S-dox conjugate, was exhibited the lowest cell viability of 60% at the physiological pH though its' efficacy dropped slightly in the artificially acidified medium. In the acidic medium preferentially, the pH stimuli conjugate displayed the highest cell viability drop from 18% compared to the pH 7.4 cell viability. However, overall, the use of stimuli controlled ligands in nano-drug delivery platforms may improve the anti-cancer efficacy even though the DLC% is low. Moreover, the stimuli triggered nanosystems may enhance the sustained drug release suggesting the low acute toxicity to healthy cells.

Author contributions

Sajini D. Hettiarachchi was responsible for synthesizing all the conjugates, running the *in vitro* drug release experiments, cell viability preliminary studies, analyzing all the data, and writing the manuscript. Emel Kirbas Cilingir and Elif S. Seven withdrew the sample in a few hours and analyzed it with UV-vis for the drug release paradigms. Emel also conducted the FTIR analysis for S–S stretching. Heidi Maklouf and Regina M. Graham were conducted the secondary cell viability studies, while Suraj paudel was conducted the calibration curves for the DLC calculations. Roger M. Leblanc, Steven

Vanni, and Regina M. graham revised the manuscript to enhance the quality.

Conflicts of interest

The authors declare no conflict of interest.

Acknowledgements

We appreciate the generous funding support given by the National Science Foundation (grant numbers: 1809060 and 2041413). Also, we extend our deepest gratitude to the Mystic Force Foundation for providing us with the funding support for cell studies.

References

1 Y. Wang and L. Chen, *Nanomedicine*, 2011, **7**, 385–402.
2 B. B. S. Cerqueira, A. Lasham, A. N. Shelling and R. Al-Kassas, *Eur. J. Pharm. Biopharm.*, 2015, **97**, 140–151.
3 A. Wicki, D. Witzigmann, V. Balasubramanian and J. Huwyler, *J. Controlled Release*, 2015, **200**, 138–157.
4 S. Zhang, J. Zou, F. Zhang, M. Elsabahy, S. E. Felder, J. Zhu, D. J. Pochan and K. L. Wooley, *J. Am. Chem. Soc.*, 2012, **134**, 18467–18474.
5 Y. Zhou, P. Y. Liyanage, D. L. Geleroff, Z. Peng, K. J. Mintz, S. D. Hettiarachchi, R. R. Pandey, C. C. Chusuei, P. L. Blackwelder and R. M. Leblanc, *ChemPhysChem*, 2018, **19**, 2589–2597.
6 S. D. Hettiarachchi, R. M. Graham, K. J. Mintz, Y. Zhou, S. Vanni, Z. Peng and R. M. Leblanc, *Nanoscale*, 2019, **11**, 6192–6205.
7 Y. Zhou, K. J. Mintz, C. Y. Oztan, S. D. Hettiarachchi, Z. Peng, E. S. Seven, P. Y. Liyanage, S. De La Torre, E. Celik and R. M. Leblanc, *Polymers*, 2018, **10**, 921–932.
8 Z. Peng, E. H. Miyanji, Y. Zhou, J. Pardo, S. D. Hettiarachchi, S. Li, P. L. Blackwelder, I. Skromne and R. M. Leblanc, *Nanoscale*, 2017, **9**, 17533–17543.
9 C. D. Walkey and W. C. Chan, *Chem. Soc. Rev.*, 2012, **41**, 2780–2799.
10 Y. H. Bae and K. Park, *J. Controlled Release*, 2011, **153**, 198–205.
11 T. Feng, X. Ai, H. Ong and Y. Zhao, *ACS Appl. Mater. Interfaces*, 2016, **8**, 18732–18740.
12 N. Dhenadhayalan, K.-C. Lin, R. Suresh and P. Ramamurthy, *J. Phys. Chem. C*, 2016, **120**, 1252–1261.
13 H. Peng, R. Dong, S. Wang, Z. Zhang, M. Luo, C. Bai, Q. Zhao, J. Li, L. Chen and H. Xiong, *Int. J. Pharm.*, 2013, **446**, 153–159.
14 K. Yang, L. Feng and Z. Liu, *Adv. Drug Delivery Rev.*, 2016, **105**, 228–241.
15 W. Fu, M. H. Mohd Noor, L. M. Yusof, T. A. T. Ibrahim, Y. S. Keong, A. Z. Jaji and M. Z. A. B. Zakaria, *J. Exp. Nanosci.*, 2017, **12**, 166–187.
16 P. Swietach, R. D. Vaughan-Jones, A. L. Harris and A. Hulikova, *Philos. Trans. R. Soc., B*, 2014, **369**, 20130099–20130107.
17 M. Stubbs, P. M. McSheehy, J. R. Griffiths and C. L. Bashford, *Mol. Med. Today*, 2000, **6**, 15–19.
18 V. Estrella, T. Chen, M. Lloyd, J. Wojtkowiak, H. H. Cornnell, A. Ibrahim-Hashim, K. Bailey, Y. Balagurunathan, J. M. Rothberg and B. F. Sloane, *Cancer Res.*, 2013, **73**, 1524–1535.
19 R. A. Gatenby, E. T. Gawlinski, A. F. Gmitro, B. Kaylor and R. J. Gillies, *Cancer Res.*, 2006, **66**, 5216–5223.
20 D. Fukumura, L. Xu, Y. Chen, T. Gohongi, B. Seed and R. K. Jain, *Cancer Res.*, 2001, **61**, 6020–6024.
21 J. W. Wojtkowiak, J. M. Rothberg, V. Kumar, K. J. Schramm, E. Haller, J. B. Proemsey, M. C. Lloyd, B. F. Sloane and R. J. Gillies, *Cancer Res.*, 2012, **72**, 3938–3947.
22 X. Zhang, F. G. Wu, P. Liu, N. Gu and Z. Chen, *Small*, 2014, **10**, 5170–5177.
23 A. L. Ortega, S. Mena and J. M. Estrela, *Cancers*, 2011, **3**, 1285–1310.
24 Y. Xianyu, Y. Xie, N. Wang, Z. Wang and X. Jiang, *Small*, 2015, **11**, 5510–5514.
25 Y. Guo, H. Wang, Y. Sun and B. Qu, *Chem. Commun.*, 2012, **48**, 3221–3223.
26 R. Cheng, F. Feng, F. Meng, C. Deng, J. Feijen and Z. Zhong, *J. Controlled Release*, 2011, **152**, 2–12.
27 L. Liu and P. Liu, *Front. Mater. Sci.*, 2015, **9**, 211–226.
28 J. B. Matson and S. I. Stupp, *Chem. Commun.*, 2011, **47**, 7962–7964.
29 V. Rao N, S. Mane, A. Kishore, J. Das Sarma and R. Shunmugam, *Biomacromolecules*, 2012, **13**, 221–230.
30 X. Hu, S. Liu, Y. Huang, X. Chen and X. Jing, *Biomacromolecules*, 2010, **11**, 2094–2102.
31 J. Xu, B. Qin, S. Luan, P. Qi, Y. Wang, K. Wang and S. Song, *J. Bioact. Compat. Polym.*, 2018, **33**, 119–133.
32 T.-M. Sun, Y.-C. Wang, F. Wang, J.-Z. Du, C.-Q. Mao, C.-Y. Sun, R.-Z. Tang, Y. Liu, J. Zhu and Y.-H. Zhu, *Biomaterials*, 2014, **35**, 836–845.
33 X. Wang, L. Wang, S. Yang, M. Zhang, Q. Xiong, H. Zhao and L. Liu, *Macromolecules*, 2014, **47**, 1999–2009.
34 L. Yang, Z. Wang, J. Wang, W. Jiang, X. Jiang, Z. Bai, Y. He, J. Jiang, D. Wang and L. Yang, *Nanoscale*, 2016, **8**, 6801–6809.
35 Y.-C. Wang, F. Wang, T.-M. Sun and J. Wang, *Bioconjugate Chem.*, 2011, **22**, 1939–1945.
36 A. Cunningham, N. R. Ko and J. K. Oh, *Colloids Surf., B*, 2014, **122**, 693–700.
37 M. Chen, J. Hu, L. Wang, Y. Li, C. Zhu, C. Chen, M. Shi, Z. Ju, X. Cao and Z. Zhang, *Sci. Rep.*, 2020, **10**, 1–12.
38 S. Li, L. Wang, C. C. Chusuei, V. M. Suarez, P. L. Blackwelder, M. Micic, J. Orbulescu and R. M. Leblanc, *Chem. Mater.*, 2015, **27**, 1764–1771.
39 P. Kurnaz, C. Y. Ataol, H. Bati and O. Buyukgungor, *Mol. Cryst. Liq. Cryst.*, 2016, **634**, 61–72.
40 V. Maulik, S. Jennifer and J. Teruna, *Curr. Protein Pept. Sci.*, 2009, **10**, 614–625.

41 B. Wang and Z. Cao, *Chem. – Eur. J.*, 2011, **17**, 11919–11929.
42 K. E. Kim, J. Li, R. H. Grubbs and B. M. Stoltz, *J. Am. Chem. Soc.*, 2016, **138**, 13179–13182.
43 M. Szostak and J. Aube, *Chem. Rev.*, 2013, **113**, 5701–5765.
44 J. Artacho, E. Ascic, T. Rantanen, J. Karlsson, C. J. Wallentin, R. Wang, O. F. Wendt, M. Harmata, V. Snieckus and K. Wärnmark, *Chem. – Eur. J.*, 2012, **18**, 1038–1042.
45 S. Mahesh, K.-C. Tang and M. Raj, *Molecules*, 2018, **23**, 2615–2657.
46 M. Huo, J. Yuan, L. Tao and Y. Wei, *Polym. Chem.*, 2014, **5**, 1519–1528.
47 W. Chen, P. Zhong, F. Meng, R. Cheng, C. Deng, J. Feijen and Z. Zhong, *J. Controlled Release*, 2013, **169**, 171–179.
48 D. S. Backos, C. C. Franklin and P. Reigan, *Biochem. Pharmacol.*, 2012, **83**, 1005–1012.